

Quantum information with quantum-like bits

Graziano Amati, Gregory D. Scholes

Department of Chemistry, Princeton University, Princeton, NJ 08544, USA.

(Dated: 30 January 2025)

In previous work we have proposed a construction of quantum-like bits that could endow a large synchronizing classical system, for example of oscillators, with quantum-like function that is not compromised by decoherence. In the present paper we investigate further this platform of quantum-like states. Firstly, we discuss a general protocol on how to construct classical synchronizing networks that allow for emergent states. We then study how gates can be implemented on those states. This suggests the possibility of quantum-like information processing on a special class of many-body classical systems. Finally, we show that our approach allows for non-Kolmogorov interference, a feature that separates our model from a classical probabilistic system. This paper aims to explore the mathematical structure of quantum-like resources distilled from classical synchronizing systems, and shows how arbitrary gates can be implemented by manipulating many-body correlations.

I. INTRODUCTION

The present noisy-intermediate scale quantum (NISQ) era of quantum devices is witnessing the successful implementation and test of diverse quantum algorithms on medium-size quantum hardware, from search on unsorted databases,¹ to variational quantum algorithms,² to simulations of open quantum dynamics.³ However, hardware of at least hundreds of thousands of physical qubits, way beyond the current engineering capabilities, is needed to obtain practical quantum advantage. This involves storing and processing the information volume required by the most challenging and relevant computational problems.⁴ The critical issue limiting the scalability of quantum resources is the buildup of uncontrolled noise and dissipation, leading to loss of coherence and fidelity.^{5–7}

In parallel with quantum engineering advancements, ongoing research investigates whether classical computing resources can continue to play a key role in information processing. For example, tensor network simulations have been shown to outperform the most advanced quantum processors in selected algorithms.⁸ Efficient quantum-inspired protocols have been successfully developed, leveraging advancements in information processing derived from quantum logic.⁹

A large class of regular graphs encodes the correlations required to identify robust collective states. This general feature can be exploited for a variety of applications. For example, we discussed in Ref. 10 how this principle can support the engineering of molecular delocalization. The same reference, along with Refs. 11 and 12, offers the interested reader background information on the mathematical formalism of regular and expander graphs, as well as their spectral properties. In the spirit of quantum-inspired computing, we showed in recent work that network correlations can serve as resources for quantum information processing.^{13–16} We focused, in particular, on many body systems whose correlations obey the graph structure shown in panel a) of Fig. 1. Here, two densely connected regions (in blue) of a network are mutually in-

teracting via sparse links (in red). A spectral analysis of this class of graphs highlights the presence of two isolated emergent states. These can be clearly distinguished from a broad band of states arising from random network configurations (dashed lines in the spectra of Fig. 1). The robustness of emergent states against noise appears to be a direct consequence of synchronization.^{13,14} This intriguing feature is related to the occurrence of classical synchronization phenomena.^{17–20} We showed in Ref. 15 that the emergent states of connected expander graphs are isomorphic to the Hilbert space of a qubit. This led us to introducing the notion of quantum-like (QL) bits within the context of classically-synchronizing networks. In Ref. 16 we built on these results and proposed a general framework to construct resources for multiple QL bits. In particular, we showed that the Cartesian product (\square) of N_{QL} bipartite graphs obeys the same dimensionality of a register of N_{QL} qubits [see panel b) of Fig. 1].

In the present paper, we build on the foundational work of Ref. 14–16, by proposing a self-contained formalization of the concepts of QL states and gates and their application to classical many-body systems. As sketched in Fig. 1, we present a framework to map the emergent states of a classical synchronizing network of oscillators onto a qubit Hilbert space. We highlight a connection between emergent states and steady-state synchronization dynamics, and we show that the latter is robust even in presence of stochastic disorder in the network. This makes the emergent states viable candidates for QL information processing, which we implement by transforming the matrix of the two-body correlations between the oscillators. Our analysis is general and applies to any classical system whose two-body correlations align with the network structures discussed later in this paper. However, to make the approach more concrete, we provide explicit examples in this manuscript by examining the synchronization dynamics of the Kuramoto model. This is a non-symplectic classical system consisting of a network of nonlinear oscillators, whose collective properties have been extensively explored in the literature.^{21–24}

Our approach leads to a natural correspondence be-

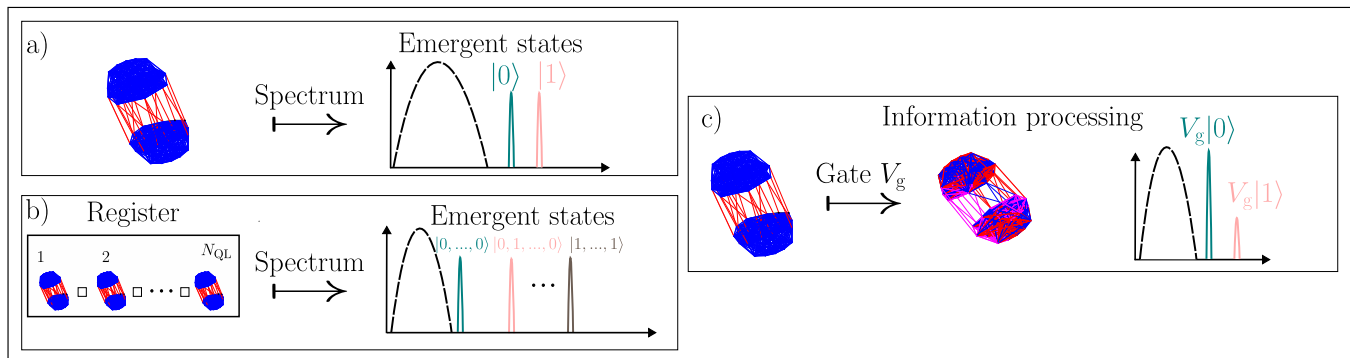


FIG. 1: Illustration of the main concepts presented in this paper and in prior work by the authors.^{15,16} a) Many body systems consisting of networks of oscillators can easily exhibit classical synchronization phenomena. By structuring two-body correlations into two densely connected regions (blue) weakly interacting through sparse links (red), synchronization gives rise to pairs of emergent states. These states are well-distinguishable from a large band of random states at lower energies (dashed line in the sketch of the spectrum). In Ref. 15 we proposed a map from emergent states to the computational basis of a qubit. b) In Ref. 16, we demonstrated that the emergent states of the Cartesian product of a set of synchronizing graphs scale with the same dimensionality of a qubit system. In this paper, we expand over these concepts by bridging classical synchronization dynamics and the QL formalism. c) Additionally, we elaborate on the concept of QL information processing, and how this connects to steady-state synchronization dynamics. We show that operations on graphs, implemented through suitable transformations of their edges, are equivalent to gate transformations \hat{V}_g applied directly to the emergent states.

tween “QL gates” transformations and the steady states of the classical oscillatory dynamics. Additionally, we propose a variety of experimental resources that can be utilized to test the formalism. This supports the applicability of the approach for information protocols involving low-dimensional Hilbert spaces, where the exponentially large complexity of the classical phase space can be handled by available experimental resources. Finally, we connect our perspective to the QL probabilistic framework developed by Khrennikov.^{25–27} This theory formalizes the notion that genuine quantum systems are not required to process information in a QL way. Instead, to observe nonclassical interference it is sufficient to construct a contextual probability theory involving suitable notions of QL states, observables, and projective measurements.

The present paper is structured as follows. In Section II A we summarize our previous work describing how to construct a single-QL-bit Hilbert space. In Section II B

we discuss its generalization to higher dimensions, and we show explicitly in Section II B 2 how to construct Bell states for two QL bits. In Section III we show the fundamental role of emergent states in the synchronizing dynamics of the Kuramoto model as a paradigmatic classical system of synchronizing oscillators. In Section IV we study the action of a complete set of QL gates, and we provide concrete examples of their action. In Section VI, we present a set of axioms that enables us to define a QL probabilistic theory in our approach. In particular, we highlight the presence of a nonclassical interference term in the relation between total and conditional probabilities, specific to non-Kolmogorovian contextual probabilistic models.²⁷ Finally, in Section V, we propose a variety of experimental resources that could be utilized to implement and verify experimentally our formalism.

In conjunction with Refs. 14–16, this work provides the mathematical foundation for a rigorous approach to QL information processing from classical many-body synchronizing systems.

II. QUANTUM-LIKE BITS

In this section we derive a mapping from the emergent states of classical networks to the Hilbert space of interacting QL bits. While the concept has been already elucidated in Ref. 15, here we lay out a more formal description. The present analysis provides a complete description of the axioms of states and operators in quantum mechanics, within the notation of the emergent states.

Later in the paper we show the direct connection between this abstract approach and the dynamics of many-body classical systems.

A. Isolated system

Let us consider two classical many-body systems with pairwise interactions between the elementary con-

stituents. The pair-wise interactions can be mapped onto two graphs G_1 and G_2 . Here, we assume here that both graphs involve the same number of vertices, N_G , and we label by A_1 and A_2 the related adjacency matrices. Also, we consider at this stage undirected simple graphs, without loops (while in the paper we will discuss graph transformations that break these symmetries). The adjacency matrix for this class of graphs is symmetric with entries either 0 or 1 and null diagonal. Additionally, we assume an isotropic structure for all two-body interactions, such that the valence of the graphs is constant and equal to k .²⁸ In particular,

$$\sum_{i=1}^{N_G} [A_n]_{ij'} = \sum_{j=1}^{N_G} [A_n]_{i'j} = k, \quad \forall i', j' = 1, \dots, N_G, \quad (\text{II.1})$$

and $n = 1, 2$. A key property of these subgraphs is that they exhibit an emergent state—a common feature of Erdős-Renyi random graphs and expander families, such as the k -regular graphs.^{15,29,30} The direct sum of the two adjacency matrices is

$$A_1 \oplus A_2 = \begin{bmatrix} A_1 & \mathbb{0}_{N_G} \\ \mathbb{0}_{N_G} & A_2 \end{bmatrix}, \quad (\text{II.2})$$

where we labeled by $\mathbb{0}_{N_G} \in M_{N_G}(\mathbb{N})$ the null matrix on the off-diagonal blocks. As proposed in Ref. 15, we define a QL bit resource by switching on an interaction between the two subgraphs, and define the resource

$$\mathcal{R} = \begin{bmatrix} A_1 & C \\ C^\top & A_2 \end{bmatrix}, \quad (\text{II.3})$$

involving a coupling matrix C . Note that C does not represent a simple graph by itself, i.e. it is in general non-symmetric, and it can admit diagonal entries connecting corresponding vertices in A_1 and A_2 . Conversely, Eq. (II.3), being overall symmetric and loop-free, describes a simple undirected graph. We sample C by randomly assigning 1 to $N_C \leq N_G^2$ of its entries. This matrix is chosen to be regular with valency $l = N_C/N_G$ [similarly to Eq. (II.1)]. Equation (II.3) represents the fundamental resource used to build an isolated QL bit.¹⁵

To better describe the structure of the graphs that are suitable resources for our QL platform, we show in Fig. 2 four instances of Eq. (II.3) for increasing values of l , as specified in the captions. The case $l = 0$ corresponds to uncoupled regular graphs, as in Eq. (II.2). By increasing l , we strengthen the coupling between the two subgraphs. For $l = k$, Eq. (II.3) turns into a regular matrix with total valency $2k$, with the same density of both intra- and cross-subgraphs edges.

As discussed in Refs. 14 and 15, resources with structure as in Eq. (II.3) are particularly appealing for information processing. In fact, these resources allow for emergent states associated to distinguishable eigenvalues, well isolated from a large band of random states. By mapping the states associated to those peaks onto a Hilbert space, we obtain a platform for information processing that can be controlled by network manipulation.

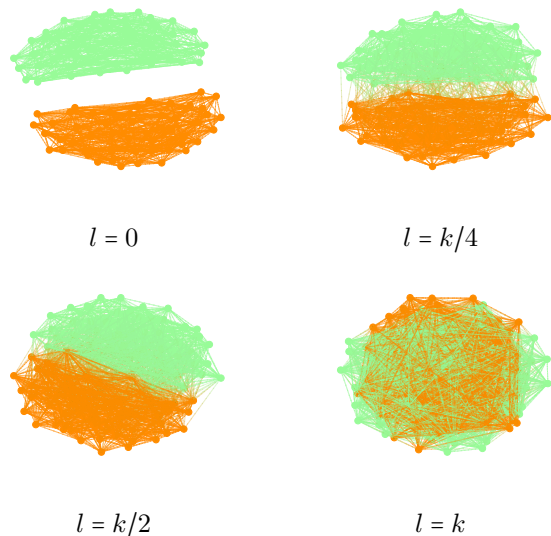


FIG. 2: Graphs associated to the resource Eq. (II.3), for increasing values of the valency l of the coupling matrix C , as specified in the captions. l is given here in units of the valency k of the subgraphs A_1 (light green/light) and A_2 (dark orange/dark). The other parameters are fixed to $N_G = 50$ and $k = 20$.

We will elaborate on these important concepts further in the manuscript.

We study the spectral properties of the resources by plotting in Fig. 3 the distribution $\rho(\lambda)$ of the eigenvalues of Eq. (II.3) for increasing values of the valency l of C . Results are shown from $l = 0$ (blue/dark) to $l = N_G$ (yellow/light). The other parameters are fixed to $N_G = 100$ and $k = 25$. The emergent states can be identified for each l from the isolated sharp peaks in the spectrum. For $l = 0$ we observe a single isolated line associated to the two-fold degenerate eigenvalue $\lambda = k = 25$ (red markers). As the valency l increases, this emergent eigenvalue split into two, and the peaks shift to $\lambda_{\pm} = k \pm l$. We track the “ballistic” evolutions of the eigenvectors as a function of the coupling valency l in the inset of Fig. 3. Here, the largest and second largest eigenvalues are shown as squared and dotted markers, respectively. While the value of the largest eigenvalue increases linearly for arbitrary l , we observe that the second largest eigenvalue plateaus at values close to $\tilde{\lambda} = 2\sqrt{k} - 1$. This barrier is defined by the radius of the Wigner semicircle distribution for a graph of order k , shown as a black dashed line in the figure.^{31,32} This portion of the spectrum is populated by random low-frequency states, whose high density makes them hardly distinguishable.^{13–15} From the present analysis we infer that, by fixing $l = (k - \tilde{\lambda})/2$, both the distance between the two emergent eigenvalues and between those and the dark states are maximized. As elucidated in Ref. 14 and 15, this analysis offers valuable insight for creating well-resolved and easily distinguishable

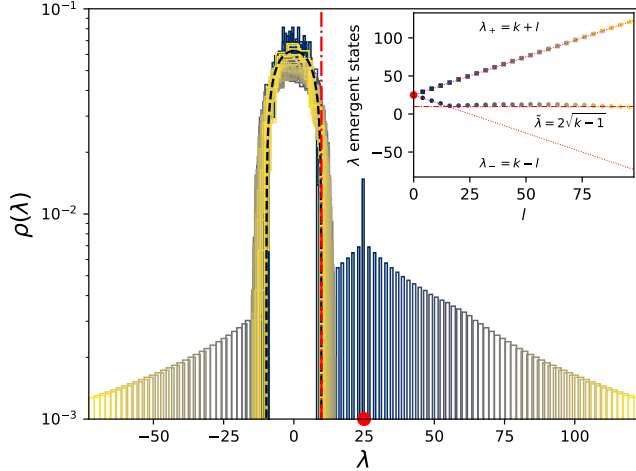


FIG. 3: Main panel: distribution of the eigenvalues λ of the QL-resource Eq. (II.3), for increasing values of the order l of the coupling matrix C , from $l = 0$ (blue/dark) to $l = N_G$ (yellow/light). Inset: largest and second largest eigenvalues of the spectrum as a function of l , with the same color code as in the main panel. We fix here $N_G = 100$ and $k = 25$.

emergent states for quantum information purposes.

We discuss now how to construct the Hilbert space $\mathcal{H}^{(1)}$ of an isolated QL qubit from coupled regular graphs, with adjacency matrices with structure as in Eq. (II.3). In particular, we define the mapping

$$\psi_{\downarrow} = \frac{1}{\sqrt{2}} \begin{pmatrix} a_1 \\ -a_2 \end{pmatrix} \mapsto |\downarrow\rangle, \quad \psi_{\uparrow} = \frac{1}{\sqrt{2}} \begin{pmatrix} a_1 \\ a_2 \end{pmatrix} \mapsto |\uparrow\rangle \quad (\text{II.4})$$

where a_i is the normalized eigenvector associated to the largest eigenvalue of A_i . As both the A_i 's and C are exactly regular, then $a_i = (1, \dots, 1)^T / \sqrt{2N_G}$ are vectors with constant weights. We keep, however, the notation general, to account for possible structural disorder in the network leading to this break of symmetry. The vectors ψ_{σ} , $\sigma \in \{\downarrow, \uparrow\} \equiv \mathcal{S}$, are eigenvectors of Eq. (II.3) with eigenvalues $\{k-l, k+l\}$, respectively. Note that in prior work we used the intention of the QL bit construction to represent explicitly the basis of the subgraphs, so that the emergent state a_1 of the graph with adjacency matrix A_1 represents $|\downarrow\rangle$, and similarly a_2 represents $|\uparrow\rangle$.^{15,16} Equation (II.4) describes another basis choice, equally valid. The present approach establishes a direct connection between the computational basis and the emergent states of the composite graph described by Eq. (II.3). In the following we show that the mapping in Eq. (II.4) leads to a well-defined Hilbert space. First of all, it is straightforward to show that the ψ_{σ} 's are mutually orthogonal

and normalized:

$$\begin{aligned} \langle \psi_{\sigma}, \psi_{\sigma'} \rangle &= \sum_{i=1}^{2N_G} \psi_{\sigma,i}^* \psi_{\sigma',i} = \frac{1}{2} (|a_1|^2 + (2\delta_{\sigma\sigma'} - 1)|a_2|^2) \\ &= \delta_{\sigma\sigma'} \mapsto \langle \sigma | \sigma' \rangle, \end{aligned} \quad (\text{II.5})$$

where $\sigma, \sigma' \in \mathcal{S}$. Operators acting on Eq. (II.4) are expressed in terms of the matrices in $M_{2N_G}(\mathbb{R})$

$$\Psi_{\sigma\sigma'} = \psi_{\sigma} \otimes \psi_{\sigma'}^{\dagger} \mapsto |\sigma\rangle \langle \sigma'|. \quad (\text{II.6})$$

As it would be expected in an abstract Hilbert space, the maps in Eq. (II.6) combine according to the rule

$$\Psi_{\sigma\sigma'} \Psi_{\pi\pi'} = \Psi_{\sigma\pi'} \langle \psi_{\sigma'}, \psi_{\pi} \rangle, \quad (\text{II.7})$$

and they transform under Hermitian conjugation as $\Psi_{\sigma\sigma'}^{\dagger} = \Psi_{\sigma'\sigma}$.

In this section we summarized a list of prescriptions for defining a mapping from a bipartite graph to the Hilbert space of a single qubit, and related properties.^{15,16} In the next Section II B we expand on an idea proposed in Ref. 16, to represent entanglement and superposition by coupling together multiple graph resources. Formal derivations on how to implement information processing and define a QL probabilistic model in this framework, follow in the later Sections IV and VI, respectively.

B. Many-body system

1. Formalism

Various representations of the quantum states are possible with respect to classical network structures. For a small number of QL bits the representation defined in Ref. 15 is useful. In that work the Bell states, involving two QL bits, are designed to give insight on proof-of-principle examples of entanglement. In Ref. 16 we propose a formal representation of states applicable to an arbitrary number of QL bits. This is based on the Cartesian product of single-QL-bit graphs. Consistently with that work, we define here as a simple generalization of Eq. (II.3) the resource for a system of N_{QL} bits

$$\mathcal{R} = \sum_{q=1}^{N_{\text{QL}}} \left[\bigotimes_{p=1}^{q-1} \mathbb{1}_{2N_G} \right] \otimes \mathcal{R}^{(q)} \otimes \left[\bigotimes_{p'=q+1}^{N_{\text{QL}}} \mathbb{1}_{2N_G} \right], \quad (\text{II.8})$$

where each $\mathcal{R}^{(q)}$ has the structure shown in Eq. (II.3). Equation (II.8) is the adjacency matrix of the Cartesian product graph¹⁶

$$\mathcal{G} = \bigboxplus_{q=1}^{N_{\text{QL}}} \mathcal{G}^{(q)}. \quad (\text{II.9})$$

Here, $\mathcal{G}^{(q)}$ is the single-QL-bit graph with adjacency matrix $\mathcal{R}^{(q)}$. The tensors

$$\psi_{\sigma} = \bigotimes_{q=1}^{N_{\text{QL}}} \psi_{\sigma^{(q)}} \mapsto \bigotimes_{q=1}^{N_{\text{QL}}} |\sigma^{(q)}\rangle = |\sigma\rangle, \quad (\text{II.10})$$

are eigenvectors of Eq. (II.8). Here, different basis elements are labeled using the multi-index $\sigma = \{\sigma^{(1)}, \dots, \sigma^{(N_{\text{QL}})}\} \in \mathcal{S}$, where $\mathcal{S} = \mathcal{S}^{N_{\text{QL}}}$. The components of Eq. (II.10) are expressed via the multi-index $\mathbf{i} = \{i^{(1)}, \dots, i^{(N_{\text{QL}})}\}$ as

$$[\psi_{\sigma}]_{\mathbf{i}} = \prod_{q=1}^{N_{\text{QL}}} \psi_{\sigma^{(q)}, i^{(q)}}. \quad (\text{II.11})$$

As discussed after Eq. (II.4), each $\psi_{\sigma^{(q)}}$, with $\sigma^{(q)} \in \mathcal{S}$, is associated to one of the eigenvalues $k \pm l$ of $\mathcal{R}^{(q)}$. Let us label this eigenvalue $\lambda_{\sigma^{(q)}}$. The action of \mathcal{R} on ψ_{σ} is then given by

$$\begin{aligned} \mathcal{R}\psi_{\sigma} &= \sum_{q=1}^{N_{\text{QL}}} \left[\bigotimes_{p=1}^{q-1} \psi_{\sigma^{(p)}} \right] \otimes [\mathcal{R}^{(q)} \psi_{\sigma^{(q)}}] \otimes \left[\bigotimes_{p'=q+1}^{N_{\text{QL}}} \psi_{\sigma^{(p')}} \right] \\ &= \sum_{q=1}^{N_{\text{QL}}} \lambda_{\sigma^{(q)}} \psi_{\sigma} = \lambda_{\sigma} \psi_{\sigma}, \end{aligned} \quad (\text{II.12})$$

where

$$\lambda_{\sigma} = \sum_{q=1}^{N_{\text{QL}}} \lambda_{\sigma^{(q)}}^{(q)}. \quad (\text{II.13})$$

Equations (II.12) and (II.13) tell us that the spectrum of the resource \mathcal{R} of N_{QL} QL bits will involve peaks corresponding to sums of the emergent eigenvalues of each $\mathcal{R}^{(q)}$.¹⁶

In analogy to Eq. (II.5) for $N_{\text{QL}} = 1$, the states in Eq. (II.10) define an orthonormal basis for \mathcal{H} according to the scalar product defined by

$$\begin{aligned} \langle \psi_{\sigma}, \psi_{\sigma'} \rangle &= \frac{1}{2^{N_{\text{QL}}}} \prod_{q=1}^{N_{\text{QL}}} \left[|a_1^{(q)}|^2 + (2\delta_{\sigma^{(q)}, \sigma'^{(q)}} - 1) |a_2^{(q)}|^2 \right] \\ &= \prod_{q=1}^{N_{\text{QL}}} \delta_{\sigma^{(q)}, \sigma'^{(q)}} = \prod_{q=1}^{N_{\text{QL}}} \langle \sigma^{(q)} | \sigma'^{(q)} \rangle. \end{aligned} \quad (\text{II.14})$$

Similarly, we extend the mapping of operators in Eq. (II.6) to

$$\Psi_{\sigma, \sigma'} = \psi_{\sigma} \otimes \psi_{\sigma'}^{\dagger} \mapsto \bigotimes_{q=1}^{N_{\text{QL}}} |\sigma_q^{(q)} \rangle \langle \sigma'_q{}^{(q)}| = |\sigma \rangle \langle \sigma'|, \quad (\text{II.15})$$

with components

$$[\Psi_{\sigma, \sigma'}]_{\mathbf{i}, \mathbf{j}} = \prod_{q=1}^{N_{\text{QL}}} \psi_{\sigma^{(q)}, i^{(q)}} \psi_{\sigma'^{(q)}, j^{(q)}}^*. \quad (\text{II.16})$$

The Hermitian conjugate of Eq. (II.15) is defined such that

$$[\Psi_{\sigma, \sigma'}^{\dagger}]_{\mathbf{i}, \mathbf{j}} = \prod_{q=1}^{N_{\text{QL}}} \psi_{\sigma'^{(q)}, j^{(q)}}^* \psi_{\sigma^{(q)}, i^{(q)}} = [\Psi_{\sigma', \sigma}]_{\mathbf{i}, \mathbf{j}}, \quad (\text{II.17})$$

and we generalize Eq. (II.7) to

$$\Psi_{\sigma\sigma'} \Psi_{\pi\pi'} = \Psi_{\sigma\pi'} \langle \psi_{\sigma'}, \psi_{\pi} \rangle. \quad (\text{II.18})$$

The mapping discussed here provides a general description of state vectors, entanglement and operators constructed from the emergent states of an arbitrary number of QL bits. In the next Section II B 2 we show explicitly, as an example, how to construct maximally entangled Bell states for $N_{\text{QL}} = 2$.

2. Example: Bell states

Here, we study the spectral properties of two-QL-bit resources, and we show how to construct entangled Bell states with them. Equation (II.8) in this case simplifies to

$$\mathcal{R} = \mathcal{R}^{(1)} \otimes \mathbb{1}_{2N_G} + \mathbb{1}_{2N_G} \otimes \mathcal{R}^{(2)}. \quad (\text{II.19})$$

The spectrum $\rho(\lambda)$ of a resource with structure as in Eq. (II.19) is shown in Fig. 4 for the system parameters $N_G = 16$, $k = 6$ and $l = 1$. To improve the smoothness of all distributions, we average over a number of $N_{\text{samp}} = 10^3$ realizations of random regular graphs. The black curve corresponds to the direct (dir.) calculation from the eigenvalues of Eq. (II.19). An alternative approach to calculate the spectrum is possible, by observing that each eigenvalue λ_i of Eq. (II.19) can be expressed as a sum $\lambda_i = \lambda_j^{(1)} + \lambda_k^{(2)}$, where the $\lambda_m^{(q)}$'s are eigenvalues of $\mathcal{R}^{(q)}$, $q = 1, 2$.¹⁶ We can therefore calculate the spectrum of Eq. (II.19) via the convolution

$$\rho(\lambda) = \int_{-\infty}^{+\infty} dx \rho^{(1)}(x) \rho^{(2)}(\lambda - x), \quad (\text{II.20})$$

where $\rho^{(q)}(x)$ is the spectrum of a single QL bit, shown in Fig. 3. The generalization of Eq. (II.20) provides a simple recipe to construct the spectrum of a system of an arbitrary number of QL bits starting from the spectra for $N_{\text{QL}} = 1$. The distribution calculated from the convolution (conv.) Eq. (II.20), is shown as a green (light) dashed curve in Fig. 4, and it agrees satisfactorily with the direct calculation. We mark in red on the picture the isolated peaks corresponding to the emergent eigenvalues of the two-QL-bit systems. These are $\lambda_{11} = 2k + 2l$ (circle), $\lambda_{10} = \lambda_{01} = 2k$ (cross) and $\lambda_{00} = 2k - 2l$ (square). These eigenvalues are associated to the corresponding eigenvectors $\{\psi_{\sigma\sigma'}\}_{\sigma, \sigma' \in \mathcal{S}}$, defining an orthonormal basis for the Hilbert space of two QL bits. To obtain the explicit expression of the eigenvectors, it is convenient to label the eigenvectors of each QL bit as

$$\psi_{\uparrow/\downarrow}^{(1)} = \begin{pmatrix} a_1 \\ \pm a_2 \end{pmatrix}, \quad \psi_{\uparrow/\downarrow}^{(2)} = \begin{pmatrix} b_1 \\ \pm b_2 \end{pmatrix}, \quad (\text{II.21})$$

where a_i 's and b_i 's are defined as in Eq. (II.4) for the resources $\mathcal{R}^{(1)}$ and $\mathcal{R}^{(2)}$, respectively. The notation in Eq. (II.21) indicate that the upper arrow (\uparrow) on the left-hand side is associated to the positive sign on right-hand side, and similarly for \downarrow and the negative sign. With

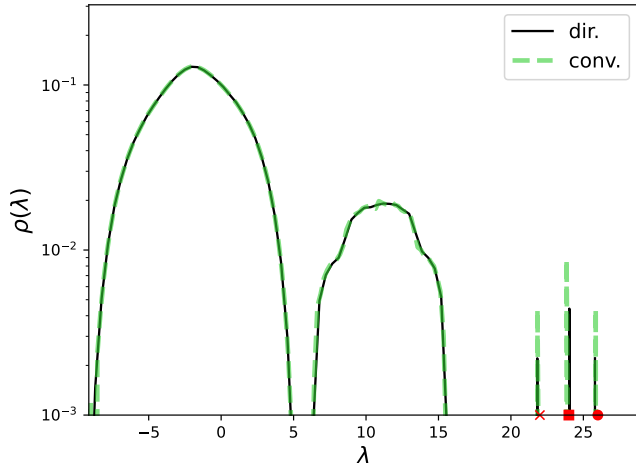


FIG. 4: Distribution of the eigenvalues of Eq. (II.19), for $N_{\text{samp}} = 10^3$ random samples of the graphs resources. The parameters of the graph are fixed here to $N_G = 16$, $k = 6$, $l = 1$. The solid black curve corresponds to the direct sampling of the eigenvalues of Eq. (II.19), while the green dashed curve is obtained from the convolution of two identical one-QL-bit distributions [Eq. (II.20)].

Eq. (II.21) we can express

$$\psi_{\uparrow, \uparrow/\downarrow} = \frac{1}{2} \begin{pmatrix} a_1 \otimes b_1 \\ \pm a_1 \otimes b_2 \\ a_2 \otimes b_1 \\ \pm a_2 \otimes b_2 \end{pmatrix}, \quad \psi_{\downarrow, \uparrow/\downarrow} = \frac{1}{2} \begin{pmatrix} a_1 \otimes b_1 \\ \pm a_1 \otimes b_2 \\ -a_2 \otimes b_1 \\ \mp a_2 \otimes b_2 \end{pmatrix}. \quad (\text{II.22a})$$

We can finally construct maximally entangled Bell states via the linear combinations

$$\Phi_{\uparrow/\downarrow}^{\text{Bell}} = \frac{1}{\sqrt{2}} (\psi_{\uparrow\uparrow} \pm \psi_{\downarrow\downarrow}), \quad (\text{II.23a})$$

$$\Psi_{\uparrow/\downarrow}^{\text{Bell}} = \frac{1}{\sqrt{2}} (\psi_{\uparrow\downarrow} \pm \psi_{\downarrow\uparrow}), \quad (\text{II.23b})$$

that is,

$$\Phi_{\uparrow}^{\text{Bell}} = \frac{1}{\sqrt{2}} \begin{pmatrix} a_1 \otimes b_1 \\ \mathbb{0}_{N_G} \\ \mathbb{0}_{N_G} \\ a_2 \otimes b_2 \end{pmatrix}, \quad \Phi_{\downarrow}^{\text{Bell}} = \frac{1}{\sqrt{2}} \begin{pmatrix} \mathbb{0}_{N_G} \\ a_1 \otimes b_2 \\ a_2 \otimes b_1 \\ \mathbb{0}_{N_G} \end{pmatrix}, \quad (\text{II.24a})$$

$$\Psi_{\uparrow}^{\text{Bell}} = \frac{1}{\sqrt{2}} \begin{pmatrix} a_1 \otimes b_1 \\ \mathbb{0}_{N_G} \\ \mathbb{0}_{N_G} \\ -a_2 \otimes b_2 \end{pmatrix}, \quad \Psi_{\downarrow}^{\text{Bell}} = \frac{1}{\sqrt{2}} \begin{pmatrix} \mathbb{0}_{N_G} \\ -a_1 \otimes b_2 \\ a_2 \otimes b_1 \\ \mathbb{0}_{N_G} \end{pmatrix}. \quad (\text{II.24b})$$

So far, we have presented general results on the QL formalism and demonstrated that the approach enables an exact mapping to the Hilbert space of a qubit system. In the following Section III, we explore how the abstract

concepts of graph resources and emergent states relate to the classical dynamics of a system of oscillators. We discuss the resilience of this approach in the presence of noise in the network correlations and highlight the critical role of emergent states in the classical synchronizing dynamics.

III. CLASSICAL SYNCHRONIZATION

Here, we investigate classical synchronization in dynamical systems of oscillators, where two-body correlations are governed by a connectivity matrix with the structure described in Eq. (II.3). Systems that align with our formalism must, as a general requirement, involve classical many-body dynamics, where the two-body couplings between degrees of freedom are governed by a connectivity matrix \mathcal{R} , as outlined in Section II. Additionally, the dynamics should guarantee that synchronization leads to a globally stable state that remains robust over long time scales. These features are satisfied by the non-symplectic dynamics of the Kuramoto model^{21–24}, which is characterized by its nonlinear equations of motion

$$\dot{\theta}_i = \omega_i + \frac{\Gamma}{2N_G} \sum_{j=1}^{2N_G} \mathcal{R}_{ij} \sin(\theta_j - \theta_i), \quad i = 1, \dots, 2N_G. \quad (\text{III.1})$$

Here, the θ_i 's are angular variables corresponding to $2N_G$ oscillators, defined on the vertices of a graph. The matrix \mathcal{R} encodes the correlations between these degrees of freedom. The ω_i 's denote the intrinsic oscillation frequencies. The time evolution of the angular variables of the model is shown in panel a) of Fig. 5. For our chosen system parameters (see caption of the figure) the system reaches a synchronized steady state, where all oscillators evolve at a uniform, constant phase. The synchronized steady state appears robust even in presence of disorder in the network, as shown in panel b) of the same figure. Here, white static disorder, with variance $\sigma = 3$ and a zero mean, is added to all nonzero entries of the adjacency matrix \mathcal{R} , originally valued at one. Despite this strong perturbation, a collective synchronization state persists at long times, with only minor phase shifts affecting small subgroups of oscillators. This observation further supports the authors' previous findings on the resilience of synchronization dynamics to noise—a property particularly appealing for robust information encoding and processing in the steady states of these classical dynamical systems.^{14–16}

To examine the role of the emergent states in the synchronization dynamics it is convenient to express the adjacency matrix through its spectral decomposition, as

$$\mathcal{R} = \sum_{\sigma \in \mathcal{S}} \lambda_{\sigma} (\psi_{\sigma} \otimes \psi_{\sigma}^{\dagger}) + \sum_{i=1}^{M-2} \tilde{\lambda}_i (\tilde{\psi}_i \otimes \tilde{\psi}_i^{\dagger}), \quad (\text{III.2})$$

where $M = (2N_G)^{N_{\text{QL}}}$ denotes the total number of states. The first term in Eq. (III.2) represents the contribution of

the emergent states ψ_σ 's. The second term corresponds to the random part of the spectrum, with eigenvalues $\tilde{\lambda}_i$'s and corresponding eigenvectors $\tilde{\psi}_i$'s. Panel b) of Fig. 5 depicts the time evolution of the Kuramoto dynamics when only the random part of the spectrum is taken into account [that is, by imposing $\lambda_\sigma \equiv 0 \ \forall \sigma \in \mathcal{S}$ in Eq. (III.2)]. In this scenario, synchronization fails to emerge, with all degrees of freedom maintaining their initial random phases throughout the entire time evolution. This highlights that the structure of two-body correlations and emergent states, encoded in the adjacency matrix \mathcal{R} , play a critical role in achieving classical synchronization. In the next Section IV, we build on these idea by exploring the connection between dynamical synchronization and information processing. This approach provides a framework for linking the steady states of classical many-body systems to quantum information protocols.

IV. QUANTUM-LIKE GATES

In this section, we explore the fundamental principles of QL information processing. In Section IV A, we formalize how the emergent states of QL resources can be systematically transformed according to arbitrary quantum gates. We further investigate the correspondence between state transformations and network resources. In Section IV B, we connect this abstract formalism to the dynamics of classical synchronization. Specifically, we demonstrate how QL gates can be practically realized in classical many-body systems of synchronizing oscillators and analyze the impact of these transformations on the long-time steady states of their dynamics.

A. Formalism

To connect the usual definition of gates acting on an abstract Hilbert space to our QL formalism, it is convenient to introduce a map U_{cb} transforming the emergent eigenvectors onto the standard computational basis. As that all elementary subgraphs in our resources [Eqs. (II.3) and (II.8)] are regular, this map can be expressed analytically by

$$U_{\text{cb}} = [V_{\text{H}} \otimes \mathbb{1}_{N_G}]^{\otimes N_{\text{QL}}}, \quad (\text{IV.1})$$

where

$$V_{\text{H}} = \frac{1}{\sqrt{2}} \begin{pmatrix} 1 & 1 \\ 1 & -1 \end{pmatrix} \quad (\text{IV.2})$$

denotes the matrix representation of the Hadamard (H) gate in the computational basis. The action of U_{cb} becomes clear for $N_{\text{QL}} = 1$, where

$$U_{\text{cb}}\psi_\uparrow = \begin{pmatrix} 1_{N_G} \\ 0_{N_G} \end{pmatrix}, \quad U_{\text{cb}}\psi_\downarrow = \begin{pmatrix} 0_{N_G} \\ 1_{N_G} \end{pmatrix}, \quad (\text{IV.3})$$

and

$$x_M = (x, \dots, x)/\sqrt{M} \in \mathbb{C}^M, \quad x \in \mathbb{C}, M \in \mathbb{N}. \quad (\text{IV.4})$$

Note that, given that all the basis subgraphs are regular, the solution to Eq. (IV.3) is independent of their local structure. We show in Appendix A that a solution for the map U_{cb} can be determined if the resources are not exactly regular, by solving numerically a linear algebra problem. We define the QL analog of any arbitrary quantum gate V_{g} by the matrix transformation

$$U_{\text{g}} = U_{\text{cb}}^{-1}(V_{\text{g}} \otimes \mathbb{1}_{N_G})U_{\text{cb}}. \quad (\text{IV.5})$$

To elucidate the action of Eq. (IV.5), let us consider a few examples. The QL maps of the identity operator (\mathcal{I}) and the three Pauli gates (X,Y,Z) are

$$U_{\mathcal{I}} = \begin{pmatrix} \mathbb{1}_{N_G} & 0_{N_G} \\ 0_{N_G} & \mathbb{1}_{N_G} \end{pmatrix}, \quad (\text{IV.6a})$$

$$U_X = \begin{pmatrix} \mathbb{1}_{N_G} & 0_{N_G} \\ 0_{N_G} & -\mathbb{1}_{N_G} \end{pmatrix}, \quad (\text{IV.6b})$$

$$U_Y = \begin{pmatrix} 0_{N_G} & i\mathbb{1}_{N_G} \\ -i\mathbb{1}_{N_G} & 0_{N_G} \end{pmatrix}, \quad (\text{IV.6c})$$

$$U_Z = \begin{pmatrix} 0_{N_G} & \mathbb{1}_{N_G} \\ \mathbb{1}_{N_G} & 0_{N_G} \end{pmatrix}, \quad (\text{IV.6d})$$

respectively. As expected, the transformations in Eq. (IV.6b) act as the standard Pauli gates:

$$U_X\psi_{\uparrow/\downarrow} = \psi_{\downarrow/\uparrow}, \quad U_Y\psi_{\uparrow/\downarrow} = \pm i\psi_{\downarrow/\uparrow}, \quad U_Z\psi_{\uparrow/\downarrow} = \pm\psi_{\uparrow/\downarrow}. \quad (\text{IV.7})$$

As another example, the QL map corresponding to the Hadamard gate transforms states in the factorized basis into superposition states:

$$U_{\text{H}}\psi_{\uparrow/\downarrow} = (V_{\text{H}} \otimes \mathbb{1}_{N_G})\psi_{\uparrow/\downarrow} = \frac{1}{\sqrt{2}}(\psi_\uparrow \pm \psi_\downarrow). \quad (\text{IV.8})$$

The formal approach proposed here applies equally to any arbitrary gates, including those outside the Clifford group. While gates outside the Clifford group break the stabilizer structure and require exponentially more resources compared to Clifford gates—which can be efficiently simulated classically—the distinction between these two classes of gates is not relevant to our framework. Our formalism is designed to be computationally exact, addressing the exponentially high cost associated with scaling QL resources, regardless of the type of gate involved. The action of the non-Clifford T-gate on the factorized basis is

$$U_{\text{T}}\psi_{\uparrow/\downarrow} = \frac{1}{2} \left[(1 + e^{i\pi/4})\psi_\uparrow + (1 - e^{i\pi/4})\psi_\downarrow \right]. \quad (\text{IV.9})$$

Finally, as an example of two-QL-bit transformation, we consider the two-QL-bit controlled NOT (CN) gate. This is defined in an abstract Hilbert space by $\hat{V}_{\text{CN}} = |\uparrow\rangle\langle\uparrow| \otimes \hat{\mathcal{I}} + |\downarrow\rangle\langle\downarrow| \otimes \hat{X}$, where $\hat{\mathcal{I}}$ and \hat{X} are the identity and the Pauli-X

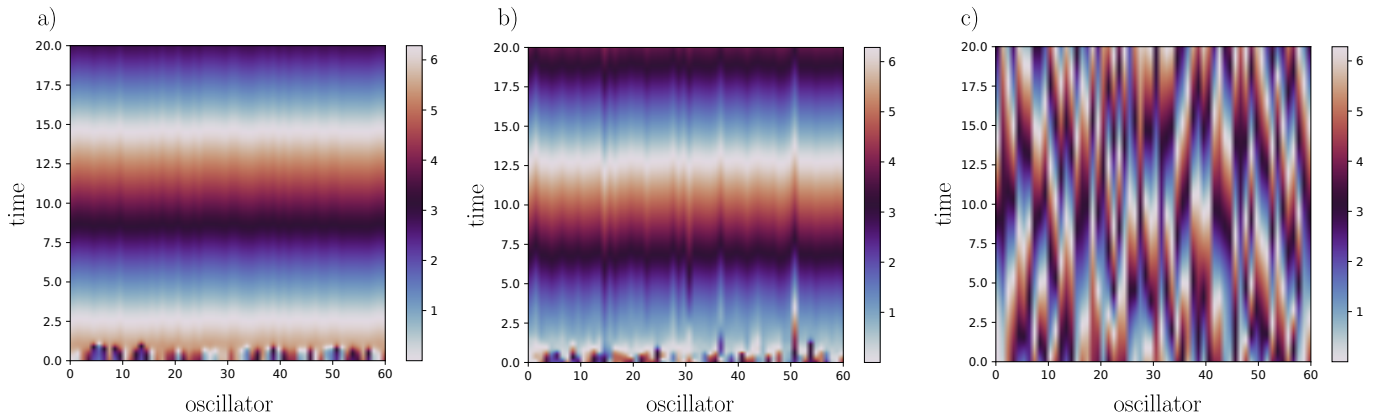


FIG. 5: a): Time evolution of a system with $2N_G = 60$ oscillators governed by the Kuramoto model [Eq. (III.1)]. The angular variables θ_i are initialized uniformly in $[0, 2\pi)$, and the intrinsic frequencies ω_i are sampled uniformly from $(0, 1)$. The coupling constant is set to $\Gamma = 10$, and the connectivity matrix \mathcal{R} is structured as a regular graph, as described in Eq. (II.3), with the valencies of the diagonal and off-diagonal blocks set to $k = 29$ and $l = 15$, respectively. b): Time evolution of the system under the same parameters and initial conditions as in a), but with disorder introduced into the connectivity matrix \mathcal{R} . Specifically, each nonzero entry of \mathcal{R} is perturbed by random white noise with zero mean and variance $\sigma = 3$. c): Dynamics of the Kuramoto model with the connectivity matrix restricted to its random components [see discussion following Eq. (III.2)]. The system parameters and initial conditions are the same as in a) and b).

operator, respectively. As expected, the transformation acts on the second QL bit of a two-QL-bit Hilbert space as either the identity or the NOT gate, depending on the control state defined by the first QL bit. In particular, the QL operator

$$U_{CN} = \frac{1}{2}(U_I + U_Z) \otimes U_I + \frac{1}{2}(U_I - U_Z) \otimes U_X \quad (\text{IV.10})$$

transforms the elements of the factorized basis as follows:

$$U_{CN}\psi_{\uparrow[\uparrow,\downarrow]} = \psi_{\uparrow[\uparrow,\downarrow]}, \quad U_{CN}\psi_{\downarrow[\uparrow,\downarrow]} = \psi_{\downarrow[\downarrow,\uparrow]}. \quad (\text{IV.11})$$

Up to this point, we have focused exclusively on the action of QL gates on states ψ_σ of the factorized basis. We can infer from those the transformation of any arbitrary state $\psi = \sum_{\sigma \in \mathcal{S}} \gamma_\sigma \psi_\sigma$, $\gamma_\sigma \in \mathbb{C}$, thanks to linearity of the map Eq. (IV.5). From a practical standpoint, it is preferable to translate these state operations onto transformations applicable directed to the graph resources. This feature is a key requirement for a future experimental validation of our formalism with experimental resources. (An extended discussion on experimental resources is provided in the next Section V). A straightforward approach in this regard is to define the unitary map

$$\mathcal{R} \mapsto \mathcal{R}_g = U_g \mathcal{R} U_g^\dagger. \quad (\text{IV.12})$$

Equation (IV.12) transforms all eigenstates of a resource consistently to the gate U_g as defined in Eq. (IV.5). This property can be easily inferred by expanding \mathcal{R} on the right-hand side of Eq. (IV.12) via the spectral decomposition in Eq. (III.2). In the next Section IV B we provide concrete examples of Eq. (IV.12), and we discuss how this network transformation affects the steady-state synchronizing solution of a system of oscillators.

B. Connection to classical synchronization

Here, we explore the relationship between gate transformations of QL resources and the synchronization of classical many-body oscillator systems. Specifically, we focus on two examples of one-QL-bit gates. In these cases, the synchronization patterns of the classical system can be directly linked to the structure of the corresponding adjacency matrices. However, our approach is general and can be extended to arbitrary QL gates without any restrictions.

The Pauli-X (NOT) gate transforms an initial resource Eq. (II.3) as follows:

$$\mathcal{R} \mapsto \mathcal{R}_X = \begin{pmatrix} A_1 & -C \\ -C^\top & A_2 \end{pmatrix}. \quad (\text{IV.13})$$

We show in panel a) of Fig. 6, the synchronization pattern in the dynamics of the Kuramoto model with correlation matrix \mathcal{R}_X . In the transformation Eq. (IV.13), the leading emergent eigenvector, associated to the largest eigenvalue $k+l$, is mapped from ψ_\uparrow to ψ_\downarrow [see Eq. (II.4)]. The change of sign in the eigenvectors corresponds to a phase shift of $\Delta\phi = \pi$ between the first and the second half of the oscillators, as shown in the figure. In the case of the Hadamard gate, resources are transformed according to

$$\mathcal{R} \mapsto \mathcal{R}_H = \begin{pmatrix} A_1 + A_2 + C + C^\top & A_1 - A_2 - C + C^\top \\ A_1 - A_2 + C - C^\top & A_1 + A_2 - C - C^\top \end{pmatrix}. \quad (\text{IV.14})$$

The sum and difference of the basis graphs A_1 and A_2 in Eq. (IV.14) highlight the fundamental role of this gate in creating a superposition state. The structure of Eq. (IV.14) encodes key information about the expected

synchronization patterns in the dynamics of the corresponding Kuramoto model, as depicted in panel b) of Fig. 6. Dephasing emerges between the first and second halves of the oscillators, primarily driven by cancellation effects in the two off-diagonal blocks, where the term $A_1 - A_2$ plays a dominant role. When $A_1 \simeq A_2$ and $C \simeq C^\top$, the off-diagonal blocks approach zero, leading to completely uncorrelated phases between the two oscillator subgroups over extended timescales. Furthermore, the second half of the oscillators, labeled by indices $i \in \{N_G, \dots, 2N_G\}$ exhibits weaker synchronization compared to the first one. This is due to the fact that the matrix norm of the lower diagonal block in Eq. (IV.14) is, on average, smaller than that of the upper diagonal block. Consequently, the second group of oscillators exhibits weaker correlations compared to the first group.

In this section, we derived general principles for mapping network resources in a manner consistent with an arbitrary set of QL gates. Additionally, we presented numerical evidence supporting the connection between QL gates and the steady-state synchronization of classical oscillator resources. In the following Section V, we explore specific examples of experimental resources that could be utilized to implement our formalism in practice.

V. EXPERIMENTAL PERSPECTIVES

So far, we have shown that the emergent states of synchronizing classical systems can be used as a basis to map the Hilbert space of a system of qubits. We discussed the primary role of emergent states in synchronization dynamics and the robustness of the latter in the presence of noise. In this section, we explore perspectives on implementing the proposed formalism using experimental physical resources. Additionally, we provide a high-level outline of computational and experimental validations that could support the further development of this framework.

For genuine quantum resources, the primary source of errors during information processing and measurement arises from uncontrolled noise. This noise can result from several factors, including external electromagnetic fields, unwanted interactions between qubits, fabrication defects, and imperfections in control protocols.^{33–37} Addressing such errors typically requires multiple measurements to accurately resolve the final state of a quantum register after computations. This can introduce significant overhead in computing protocols and hinder the scalability of the approach to larger size. Error mitigation and decoding techniques, although conceptually scalable, can result in further limitations in size and performance.^{38,39} In our approach, error correction in the presence of noise translates to enhancing the robustness of long-time classical synchronization [see the discussion on panel b) of Fig. 5]. This ensures distinct and readily measurable transformations of the steady-state dynamics. Optimal synchronization can be achieved by numer-

ically analyzing phase diagrams of synchronization indicators. For instance, in the case of the Kuramoto model, time-resolved order parameters offer clear insight into the synchronization strength.^{40,41} Parameter domains with the highest degree of synchronization can be identified as optimal candidates for experimental implementation.

In terms of resource complexity, the number of degrees of freedom required to model the synchronization dynamics of a system of N_{QL} QL bits scales exponentially with system size. Although this scaling does not impose fundamental constraints on computational studies or experimental implementations of the approach, it does limit the practical feasibility of large-scale QL algorithms. Here, we discuss a few experimental platforms that are suitable candidates for implementing QL information processing within these scaling constraints. Additionally, we identify the classes of algorithms that can be most effectively analyzed by those resources.

Implementing coupled LC circuits is a straightforward approach to implement macroscopic experimental resources that exhibit classical synchronization.^{42,43} Numerical analyses from Ref. 44 show that this class of systems can be effectively approximated by Kuramoto-type models for medium-scale systems of 60 oscillators. The couplings between the model oscillators are tuned by adjusting the transconductance values of the circuit transistors.

Spin-torque oscillators (STO) emerge as another promising candidate for implementing QL information processing.⁴⁵ STOs are nonlinear magnetic oscillators that can be integrated into nanoscale devices operating at microwave frequencies. They have the ability to synchronize in both frequency and phase with external oscillatory signals as well as with other STOs. The full magnetization dynamics of these systems, defined by the Landau-Lifshitz-Gilbert-Slonzewski (LLGS) equation, can be simplified to the Kuramoto model for small-amplitude oscillations.^{46,47} Ref. 48 demonstrates the experimental feasibility of modeling synchronizing classical systems with up to a few hundred oscillators. Beyond this scale, technical constraints arising from finite-size effects restrict the extent of achievable synchronization.

Metal-to-insulator transition (MIT) devices leverage materials that can switch between insulating and metallic (conductive) states in response to external conditions such as temperature, pressure, or electrical stimuli.⁴⁹ Research on small-scale MIT circuits has demonstrated their fundamental ability to produce classical synchronization behavior through voltage-triggered oscillatory dynamics.^{45,49,50} One limitation of current MIT devices is their low oscillation frequency, typically below 1 MHz, which hinders the ability to achieve fine-resolution synchronization and detect subtle variations in coupled oscillator behavior. However, ongoing advancements in scaling down these devices are expected to increase their oscillation frequencies, enabling more precise and time-resolved synchronization measurements.⁵¹

Building on the experimental perspectives outlined

above, it appears feasible to validate our QL-bit theory using networks of up to a hundred oscillators. Such an experimental setup would enable the implementation of proof-of-concept algorithms on systems with $N_{\text{QL}} = 2$ or $N_{\text{QL}} = 3$ QL-bits, where each QL-bit comprises a small network of 5–10 oscillators. A particularly intriguing class of quantum information processes for systems of this scale includes those that generate entanglement, such as the formation of Bell states (for $N_{\text{QL}} = 2$) and their higher-order generalizations, the Greenberger–Horne–Zeilinger (GHZ) states.^{52,53} This analysis has the potential to provide valuable insights into fundamental questions surrounding the classical-to-quantum correspondence. In particular, it could help clarify the role of non-emergent states in classical synchronizing systems as potential hidden variables within a QL-based framework for analyzing entanglement.⁵⁴

We conclude this section by presenting a practical perspective on implementing an experimental scheme to test our approach:

1. *Engineer a classical synchronizing system:* Design a system with two-body correlations represented by a graph, ensuring that its leading emergent state corresponds to the desired initial state of a QL algorithm. For example, the factorized state ψ_{\uparrow} can be associated with a Cartesian-product network structured as described in Eq. (II.8).
2. *Initialize oscillator phases:* Assign arbitrary initial conditions to the oscillator phases, ensuring they adhere to the constraint that the system’s long-time steady state achieves the expected synchronization.
3. *Allow the classical dynamics to equilibrate:* Let the system evolve until it reaches a steady state. This step requires time-resolved measurements to ensure the system has sufficient time to reach a long-time synchronized state.
4. *Perform gate operations:* Each gate operation consists of two phases: (a) transforming the correlations between the degrees of freedom and (b) allowing the system to synchronize and relax to a new emergent state.
5. *Measure the final state:* Apply projection operators to extract the state of the final resource after all gate operations have been implemented.

The proposed scheme can be tested numerically by measuring multi-time correlation functions. This process involves a series of time evolution operators defined by gate-transformed resources at different stages of a given QL algorithm. Preliminary analytical work on the Kuramoto dynamics is discussed in Appendix D [see Eq. (D.4)].

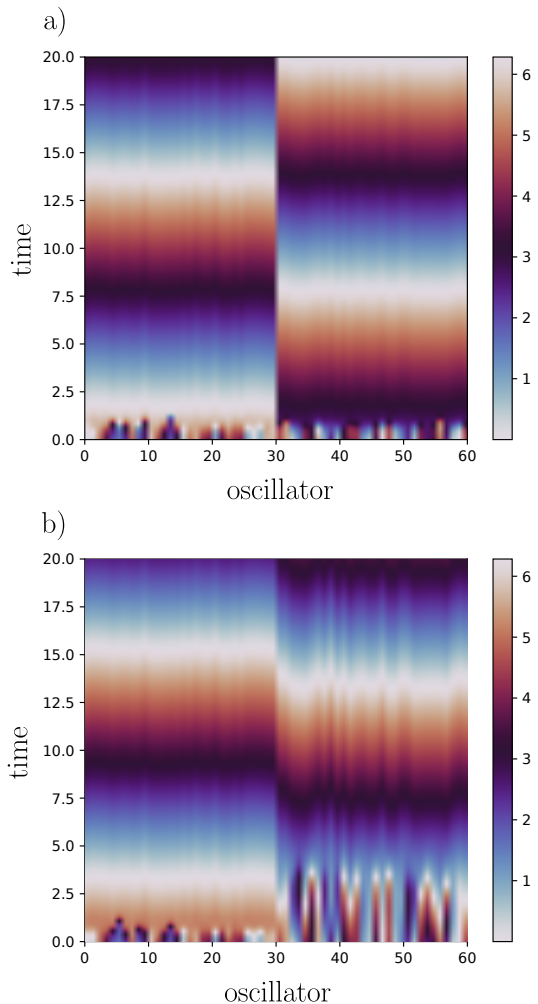


FIG. 6: a): Time evolution of a Kuramoto model where the adjacency matrix is transformed according to the mapping in Eq. (IV.12) for the Pauli-X gate ($g = X$). b): Similar to panel (a), but for the Hadamard gate ($g = H$). The same model parameters as defined in Fig. 5 are used here.

VI. QUANTUM-LIKE INTERFERENCE

In this final section, we discuss criteria that allow to introduce a notion of QL interference of probabilities in our approach. This analysis highlights that genuine quantum mechanical systems are not strictly required to build QL stochastic models provided the notions of states, observables and measurement are defined according to a given set of prescriptions.

A. Axiomatic definition

In the following we present a list of axioms, originally proposed in Ref. 27, to equip our classical network resources with a stochastic theory which mirrors the prob-

ability laws of genuine quantum mechanical systems.

Axiom 1. *QL states are represented by normalized vectors in a Hilbert space \mathcal{H} .*

States can be expressed by linear combinations of elements of the factorized basis in Eq. (II.10):

$$\psi = \sum_{\sigma \in \mathcal{S}} \alpha_{\sigma} \psi_{\sigma}. \quad (\text{VI.1})$$

Pure QL states are by definition normalized, and we establish the equivalence class $\beta\psi \sim \psi$ for $\beta \in \mathbb{C}$, $|\beta| = 1$.

Axiom 2. *QL observables are represented by self-adjoint operators on \mathcal{H} . Their action on QL states, expressed by a linear map, defines a QL measurement.*

Observables are defined in terms of linear combinations with structure

$$\mathcal{F} = \sum_{\sigma, \sigma' \in \mathcal{S}} (\gamma_{\sigma, \sigma'} \Psi_{\sigma, \sigma'} + \gamma_{\sigma', \sigma}^* \Psi_{\sigma', \sigma}), \quad \gamma_{\sigma, \sigma'} \in \mathbb{C}, \quad (\text{VI.2})$$

and fulfill the self-adjointness condition $\mathcal{F}^{\dagger} = \mathcal{F}$ [Eq. (II.17)]. The QL measurement of \mathcal{F} on a state ψ is defined by the map $\psi \mapsto \mathcal{F}\psi$.

Axiom 3. *The spectrum of a QL observable is a measurable quantity.*

An arbitrary observable \mathcal{F} , as defined in Axiom 2, is diagonalizable. Its normalized eigenvectors $\{f_{\sigma}\}_{\sigma \in \mathcal{S}}$ define an orthonormal basis of \mathcal{H} , while the corresponding eigenvalues are real and distinct. Proofs of these standard properties for the specific structure of our QL Hilbert space are given in Appendix C.

Axiom 4. *A QL probability measure defined by Born's rule is assigned to the spectrum of physical observables.*

Specifically, let us consider a generic state $\psi \in \mathcal{H}$. We define by

$$P_{\psi}(\lambda_{\sigma}^{\mathcal{F}}) = \|\Pi_{\sigma}^{\mathcal{F}} \psi\|^2 = |\langle f_{\sigma}, \psi \rangle|^2, \quad (\text{VI.3})$$

the QL probability of collapsing onto the subspace spanned by the eigenvector f_{σ} with eigenvalue $\lambda_{\sigma}^{\mathcal{F}}$, after measuring \mathcal{F} on ψ . Equation (VI.3) is expressed in terms of the projector

$$\Pi_{\sigma}^{\mathcal{F}} = f_{\sigma} \otimes f_{\sigma}^{\dagger} = (\Pi_{\sigma}^{\mathcal{F}})^2. \quad (\text{VI.4})$$

Axiom 5. *QL conditional probabilities are defined via consecutive projections onto the eigenstates of physical observables.*

In particular, let us consider two generic QL observable operators \mathcal{F} and \mathcal{G} whose spectra are defined by

$$\mathcal{F}f_{\sigma} = \lambda_{\sigma}^{\mathcal{F}} f_{\sigma}, \quad \mathcal{G}g_{\sigma} = \lambda_{\sigma}^{\mathcal{G}} g_{\sigma}. \quad (\text{VI.5})$$

For a nonzero state ψ we denote by

$$P_{\psi}(\lambda_{\sigma'}^{\mathcal{G}} | \lambda_{\sigma}^{\mathcal{F}}) = \frac{\|\Pi_{\sigma'}^{\mathcal{G}} \Pi_{\sigma}^{\mathcal{F}} \psi\|^2}{\|\Pi_{\sigma}^{\mathcal{F}} \psi\|^2} \quad (\text{VI.6})$$

the QL conditional probabilities associated to the consecutive measures of \mathcal{F} and \mathcal{G} on ψ .

We show in the next Section VIB that the QL probability model defined via Axioms 1 to 5 violates by construction Kolmogorovian classical statistics. This feature allows to introduce a notion of QL interference in our approach.^{26,55}

B. Quantum probabilities in a QL model

Before introducing a formula for the update of QL probabilities, it is instructive to briefly recall its classical correspondent, to assess analogies and differences between the two. A classical probability space is defined by the triplet $\{\Omega, \Sigma, P^{(\text{cl})}\}$, where Ω is a space of experimental outcomes, Σ the σ -algebra of its subsets, and $P^{(\text{cl})}$ a probability measure on Σ .⁵⁶ Be $\{\mathcal{A}_j\}_{j=1}^J$ a partition of Ω , i.e. a collection of J sets defined such that $A_j \neq \emptyset \forall j$, $\mathcal{A}_j \cap \mathcal{A}_{j'} = \emptyset$ for $j \neq j'$ and $\cup_{j=1}^J \mathcal{A}_j = \Omega$. $P^{(\text{cl})}$ is a positive measure on the partition elements, that is $P^{(\text{cl})}(\mathcal{A}_j) > 0 \forall j$, and it is normalized: $\sum_{j=1}^J P^{(\text{cl})}(\mathcal{A}_j) = 1$. For every $\mathcal{B} \in \Sigma$ the classical formula of total probabilities holds:⁵⁷

$$\begin{aligned} P^{(\text{cl})}(\mathcal{B}) &= P^{(\text{cl})}(\mathcal{B} \cap \cup_{j=1}^J \mathcal{A}_j) \\ &= \sum_{j=1}^J P^{(\text{cl})}(\mathcal{B} \cap \mathcal{A}_j) = \sum_{j=1}^J P^{(\text{cl})}(\mathcal{B} | \mathcal{A}_j) P^{(\text{cl})}(\mathcal{A}_j), \end{aligned} \quad (\text{VI.7})$$

where we introduced the classical conditional probability

$$P^{(\text{cl})}(\mathcal{B} | \mathcal{A}_j) = \frac{P^{(\text{cl})}(\mathcal{B} \cap \mathcal{A}_j)}{P^{(\text{cl})}(\mathcal{A}_j)}. \quad (\text{VI.8})$$

We discuss now the correspondent of Eq. (VI.7) for the present QL framework. We restrict the following analysis to couples of non-degenerate QL observables, \mathcal{F} and \mathcal{G} , whose eigenvalue problems are defined as in Eq. (VI.5). The eigenvalues of these operators are associated with a one-dimensional subspaces, which can be fixed by selecting any normalized eigenvector. In this case, the QL conditional probabilities defined in Eq. (VI.6) lose their dependence on the initial state ψ , and can be simply expressed as

$$P_{\psi}(\lambda_{\sigma'}^{\mathcal{G}} | \lambda_{\sigma}^{\mathcal{F}}) \mapsto |\langle g_{\sigma'}, f_{\sigma} \rangle|^2 \equiv P(\lambda_{\sigma'}^{\mathcal{G}} | \lambda_{\sigma}^{\mathcal{F}}). \quad (\text{VI.9})$$

Note that the probabilities in Eq. (VI.9) are symmetric, differently from their classical correspondents in Eq. (VI.8). Observables \mathcal{F} and \mathcal{G} obeying this

property for all $\sigma, \sigma' \in \mathcal{S}$ are called *symmetrically conditioned*.²⁷ This feature is a signature of *Bohr's principle of contextuality*,^{58–60} expressing the impossibility of strictly separating physical observables and the experimental context under which those are measured. The role of contextuality in a QL probabilistic framework can be highlighted by rewriting total and conditional probabilities [Eqs. (VI.3) and (VI.9), respectively], on an equal footing:

$$P(\lambda_\sigma^{\mathcal{G}}|\lambda_{\sigma'}^{\mathcal{F}}) = P_\psi(\lambda_\sigma^{\mathcal{G}})|_{\psi=f_{\sigma'}}. \quad (\text{VI.10})$$

If Eq. (VI.9) is fulfilled, Axioms 1 to 5 lead to the QL formula for probability updates^{27,61,62}

$$\begin{aligned} P_\psi(\lambda_\sigma^{\mathcal{G}}) &= \sum_{\sigma' \in \mathcal{S}} P_\psi(\lambda_{\sigma'}^{\mathcal{F}}) P(\lambda_{\sigma'}^{\mathcal{F}}|\lambda_\sigma^{\mathcal{G}}) \\ &+ \sum_{\substack{\sigma', \sigma'' \in \mathcal{S} \\ \sigma' \neq \sigma''}} \Lambda_{\sigma, \sigma', \sigma''}^\psi \left[P_\psi(\lambda_{\sigma'}^{\mathcal{F}}) P(\lambda_{\sigma'}^{\mathcal{F}}|\lambda_\sigma^{\mathcal{G}}) \right. \\ &\left. \times P_\psi(\lambda_{\sigma''}^{\mathcal{F}}) P(\lambda_{\sigma''}^{\mathcal{F}}|\lambda_\sigma^{\mathcal{G}}) \right]^{1/2}. \end{aligned} \quad (\text{VI.11})$$

An extended derivation of Eq. (VI.11) is provided in Appendix B, where we give the explicit expression of the nonclassical interference coefficient $\Lambda_{\sigma, \sigma', \sigma''}^\psi$ [Eq. (B.5)]. Information processing can be designed in a QL way, to enhance or suppress some spectral measurements compared to classical computing protocols.⁶³

As noted in Ref. 63, a significant feature of the QL probability formula Eq. (VI.11) is that it bypasses the need for calculating joint probability distributions, which are typically exponential in computational complexity. In contrast, such calculations are required for the classical updates outlined in Eq. (VI.7). This distinction relates directly to the foundational principles of quantum advantage. We intend to further investigate this property in future testing of QL algorithms.

VII. CONCLUSIONS

In this paper, we built upon the general framework developed in Refs. 14–16 to define and manipulate QL states. In Section II, we constructed a computational basis from the emergent states of many-body classical systems, whose correlations can be mapped onto synchronizing graphs. We introduced the Hilbert space for an arbitrary number of QL bits and explicitly derived the Bell states in two dimensions. In Section IV, we proposed a framework for defining quantum gates applicable to QL states and provided concrete examples of their action on many-body classical resources. Section V offers an overview of experimental platforms that could be used to implement and validate QL theory. Finally, in Section VI, we discussed that a QL notion of interference can emerge within our framework by presenting a set of axioms for interpreting QL states and observables.

Several open questions remain, presenting diverse opportunities for future research.

It can be insightful to directly relate our work to the rigorous approach to quantum non-Markovianity proposed in Refs. 64–66. In that framework a notion of conditional probabilities is defined, that accounts explicitly for the role of measurement devices on the statistics. An important feature of that formalism is that it provides an operational definition of non-Markovianity which, differently from other strategies, converges to the correct Kolmogorov conditions in the classical limit.⁶⁷

A broad class of computational approaches to open quantum systems and quantum chemistry involves a perspective somehow complementary to our approach. In particular, quantum nonadiabatic systems are often mapped onto quasiclassical models to minimize computational complexity and inexpensively approximate long-time dynamics. Accurate quasiclassical methods have been derived, by requiring that Kolmogorov probabilities [fulfilling Eq. (VI.7)] obey by construction quantum detailed balance at long times.^{68–73} It can be insightful to assess whether even more accurate quasiclassical approaches can be derived from a QL stochastic theory which approximates Eq. (VI.11) beyond the first classical term.

In this paper, we presented an early-stage analysis exploring the connection between QL gates and the many-body synchronization dynamics of oscillator systems. Specifically, we identified relationships between the structure of the adjacency matrix of the network and the synchronization patterns observed in the Kuramoto model. For future work, we aim to develop a more formal framework by deriving general expressions for multi-time correlation functions associated with network transformations induced by chains of QL gates. Additionally, we plan to investigate whether the structure of emergent QL states can be directly inferred from the synchronizing steady states and how this process is influenced by the microscopic details of the underlying classical dynamics. Future work could explore new possibilities regarding the generality of the present approach for different synchronizing dynamical systems. While this study focused on the nonlinear interactions of the Kuramoto model, it is crucial to assess the applicability of the results to a broader class of classical systems exhibiting synchronization. Extending this framework to more general models, where oscillators are represented by vectorial variables⁷⁴ or elements of a unitary group, as in the Lohe model^{23,75}, offers a promising path for further research. These generalizations enable the encoding of high-dimensional information within the phase relationships between graph nodes, potentially enhancing the modeling of complex dynamical systems.

In recent years, memcomputing has emerged as a new computational paradigm that leverages the intrinsic time-nonlocal properties of nonlinear classical dynamical systems to enable non-Boolean logic computations by exploiting memory effects within physical systems. A key

feature of memcomputing is its terminal-agnostic nature, where input and output terminals are treated equivalently. This allows self-organizing circuits to dynamically adjust and converge to equilibrium points that correspond to solutions, regardless of the terminal through which data is introduced or extracted.⁷⁶ The feasibility of the memcomputing framework has been demonstrated across various physical implementations, including oscillator-based systems.^{77,78} It can be insightful to implement a variant of our approach with flavors of memcomputing techniques, by exploiting time-nonlocality dissipative nonlinear dynamical systems, e.g. as predicted within the Nakajima–Mori–Zwanzig formalism.^{71,79–83}

The environmental implications of large-scale industrial production of quantum processors remain a topic of ongoing debate.^{84–89} Conducting an early-stage assessment of the environmental impact of various resources can provide valuable metrics to identify the most energy-efficient and scalable quantum technologies for future development. In this context, implementing energy-efficient classical circuits for QL computing offers a promising pathway toward sustainable QL-processing engineering. While our perspective does not claim to provide a definitive solution, we recognize that classical systems, despite their larger size, could serve as viable energy-efficient alternatives for specific use cases, such as small-scale, proof-of-concept analyses in fundamental research.

Finally, it can be a fascinating topic for future research to connect QL information processing introduced here to other information theories on human decision-making and psychology derived in the framework of QL contextual probability models.^{15,90–92} Implementing our formalism on brain-like neuromorphic circuits⁹³ can support theoretical and experimental investigations in this framework.

VIII. ACKNOWLEDGMENTS

We thank Debadrita Saha for useful discussions. This research was funded by the National Science Foundation under Grant No. 2211326 and the Gordon and Betty Moore Foundation through Grant GBMF7114.

Appendix A: General transformation from emergent states to the computational basis

In Section IV we discussed how a QL representation of quantum gates can be straightforwardly defined once the emergent states are mapped onto the computational basis. In general, this transformation cannot be expressed in analytic form as soon as the subgraphs defining the resources are not exactly regular. However, we show here that the problem of determining the map can be rewritten as a simple matrix inversion problem.

Firstly, it is convenient to parametrize the generaliza-

tion of Eq. (IV.1) as follows:

$$U_{\text{cb}} = \bigotimes_{q=1}^{N_{\text{QL}}} \begin{pmatrix} X^{(q)} & Y^{(q)} \\ W^{(q)} & Z^{(q)} \end{pmatrix}, \quad (\text{A.1})$$

where $X^{(q)} \in \mathbb{R}^{N_G}$ is diagonal, with components $X_{ij}^{(q)} = \delta_{ij} x_j^{(q)}$, and similarly for the other three blocks in Eq. (A.1). Equations (A.1) and (A.2) can be rewritten as the linear problem

$$x_i^{(q)} a_{1,i}^{(q)} + y_i^{(q)} a_{2,i}^{(q)} = N_G^{-1/2}, \quad (\text{A.2a})$$

$$w_i^{(q)} a_{1,i}^{(q)} + z_i^{(q)} a_{2,i}^{(q)} = 0, \quad (\text{A.2b})$$

$$x_i^{(q)} a_{1,i}^{(q)} - y_i^{(q)} a_{2,i}^{(q)} = 0, \quad (\text{A.2c})$$

$$w_i^{(q)} a_{1,i}^{(q)} - z_i^{(q)} a_{2,i}^{(q)} = N_G^{-1/2}, \quad (\text{A.2d})$$

where $q = 1, \dots, N_{\text{QL}}$, $i = 1, \dots, N_G$. Equation (A.2) is expressed in matrix form as

$$\begin{pmatrix} D_1^{(q)} & D_2^{(q)} & \mathbb{0}_{N_G} & \mathbb{0}_{N_G} \\ \mathbb{0}_{N_G} & \mathbb{0}_{N_G} & D_1^{(q)} & D_2^{(q)} \\ D_1^{(q)} & -D_2^{(q)} & \mathbb{0}_{N_G} & \mathbb{0}_{N_G} \\ \mathbb{0}_{N_G} & \mathbb{0}_{N_G} & D_1^{(q)} & -D_2^{(q)} \end{pmatrix} \begin{pmatrix} x^{(q)} \\ y^{(q)} \\ w^{(q)} \\ z^{(q)} \end{pmatrix} = \begin{pmatrix} 1_{N_G} \\ \mathbb{0}_{N_G} \\ \mathbb{0}_{N_G} \\ 1_{N_G} \end{pmatrix}, \quad (\text{A.3})$$

where $[D_n^{(q)}]_{ij} = \delta_{ij} a_{n,j}^{(q)}$, $n = 1, 2$. Equation (A.3) can be inverted to determine a solution for $(x^{(q)}, y^{(q)}, w^{(q)}, z^{(q)}) \forall q = 1, \dots, N_{\text{QL}}$, corresponding to a unique expression for U_{cb} .

Appendix B: Derivation of the quantum-like formula of total probabilities

In this appendix we derive Eq. (VI.11), describing the update of probabilities for two QL observables \mathcal{F} and \mathcal{G} , with eigenvalue problems defined as in Eq. (VI.5).

Any state vector $\psi \in \mathcal{H}$ can be expanded as

$$\psi = \sum_{\sigma \in \mathcal{S}} G_{\sigma}^{\psi} g_{\sigma} = \sum_{\sigma' \in \mathcal{S}} F_{\sigma'}^{\psi} f_{\sigma'}, \quad (\text{B.1})$$

where $F_{\sigma'}^{\psi} = \langle f_{\sigma'}, \psi \rangle$ and $G_{\sigma}^{\psi} = \langle g_{\sigma}, \psi \rangle$. We can connect the probabilities of the two observables by expressing

$$\psi = \sum_{\sigma, \sigma' \in \mathcal{S}} F_{\sigma'}^{\psi} u_{\sigma', \sigma} g_{\sigma}, \quad (\text{B.2a})$$

$$u_{\sigma', \sigma} = \langle g_{\sigma}, f_{\sigma'} \rangle, \quad (\text{B.2b})$$

which leads to the following mapping between the coefficients of ψ in the two bases:

$$G_{\sigma}^{\psi} = \sum_{\sigma' \in \mathcal{S}} F_{\sigma'}^{\psi} u_{\sigma', \sigma}. \quad (\text{B.3})$$

To relate Eq. (B.3) to QL probabilities, we define

$$F_{\sigma'}^{\psi} = e^{i\gamma_{\sigma'}^{\psi}} \sqrt{P_{\psi}(\lambda_{\sigma'}^{\mathcal{F}})}, \quad u_{\sigma', \sigma} = e^{i\Gamma_{\sigma', \sigma}} \sqrt{P(\lambda_{\sigma'}^{\mathcal{F}} | \lambda_{\sigma}^{\mathcal{G}})}, \quad (\text{B.4})$$

where $\gamma_{\sigma'}^\psi, \Gamma_{\sigma', \sigma} \in [0, 2\pi)$. By expanding the squared modulus of Eq. (B.3), we finally obtain Eq. (VI.11). This involves the phase factor

$$\Lambda_{\sigma, \sigma', \sigma''}^\psi = e^{i(\gamma_{\sigma'}^\psi - \gamma_{\sigma''}^\psi)} e^{i(\Gamma_{\sigma', \sigma} - \Gamma_{\sigma'', \sigma})}, \quad (\text{B.5})$$

which, being any other term of Eq. (VI.11) real, can be replaced by its real part:

$$\Lambda_{\sigma, \sigma', \sigma''}^\psi \mapsto \cos \left[(\gamma_{\sigma'}^\psi - \gamma_{\sigma''}^\psi)(\Gamma_{\sigma', \sigma} - \Gamma_{\sigma'', \sigma}) \right]. \quad (\text{B.6})$$

Appendix C: Spectral properties of QL observables

In this appendix we study the spectral properties of QL observables [Eq. (VI.2)], that are Hermitian operators according to the definition Eq. (II.17). In particular, we show that (i) their eigenvalues are real, (ii) eigenvectors corresponding to different eigenvalues are orthogonal, and (iii) there exists an orthonormal basis of \mathcal{H} consisting of eigenvectors. We refer here to the eigenvalues and eigenvectors of \mathcal{F} as λ_σ 's and f_σ 's, respectively.

(i) For an arbitrary f_σ

$$\langle f_\sigma, \mathcal{F} f_\sigma \rangle = \lambda_\sigma \|f_\sigma\|^2 = \langle \mathcal{F} f_\sigma, f_\sigma \rangle = \lambda_\sigma^* \|f_\sigma\|^2,$$

which implies that $\lambda_\sigma \in \mathbb{R}$.

(ii) Suppose that $\lambda_\sigma \neq \lambda_{\sigma'}$ for $\sigma \neq \sigma'$. By multiplying

$$\mathcal{F} f_\sigma = \lambda_\sigma f_\sigma, \quad (\text{C.1})$$

by $f_{\sigma'}$, we obtain

$$\begin{aligned} \langle f_{\sigma'}, \mathcal{F} f_\sigma \rangle &= \lambda_\sigma \langle f_{\sigma'}, f_\sigma \rangle \\ &= \langle \mathcal{F} f_{\sigma'}, f_\sigma \rangle \stackrel{(i)}{=} \lambda_{\sigma'} \langle f_{\sigma'}, f_\sigma \rangle, \end{aligned} \quad (\text{C.2})$$

which implies that $\langle f_{\sigma'}, f_\sigma \rangle = 0$.

(iii) Let us order the eigenvalues and eigenvectors of \mathcal{F} in increasing order, via the map

$$\sigma \mapsto n = \sum_{l=0}^{N_{\text{QL}}-1} 2^l \delta_{\sigma_l, \uparrow}. \quad (\text{C.3})$$

We denote by V_1 the set of vectors orthogonal to the eigenvector f_1 of \mathcal{F} with eigenvalue λ_1 . Note that \mathcal{F} maps V_1 onto itself, i.e., $\mathcal{F}\psi \in V_1$ for $\psi \in V_1$. In fact,

$$\langle f_1, \mathcal{F}\psi \rangle = \langle \mathcal{F} f_1, \psi \rangle = \lambda_1 \langle f_1, \psi \rangle = 0. \quad (\text{C.4})$$

The linear operator $L(\phi) = \mathcal{F}\phi$, when restricted to V_1 , is also Hermitian, and it admits an eigenvalue λ_2 with eigenvector $f_2 \in V_1$. By construction, f_2 is orthogonal to f_1 . We then define by V_2 the orthogonal complement to $\text{span}\{f_1, f_2\}$. Again, \mathcal{F} maps V_2 onto itself. By proceeding this way, we find a sequence $\{\lambda_n, f_n, V_n\}_n$, where the subspace V_n is orthogonal to $\text{span}\{f_1, \dots, f_n\}$. The sequence ends at the step of order $2^{N_{\text{QL}}}$, given that $\dim(V_n) = 2^{N_{\text{QL}}} - n$. This process allows us to define a complete set of mutually orthogonal eigenvectors.

Appendix D: Dynamics of the Kuramoto model

Here, we present a closed-form solution for the dynamics of the Kuramoto model, as described by the nonlinear equations of motion in Eq. (III.1). Our approach follows the methods outlined in Refs. 22 and 94. This analysis offers a practical framework for implementing the dynamics of the model efficiently, without the need for explicitly integrating the equations of motion, making it applicable to a broad range of synchronizing networks. Additionally, this work can serve as a starting point for future analytical studies exploring the role of emergent states in synchronization processes.

If the coupling matrix \mathcal{R} is real, it is convenient to subtract from Eq. (III.1) an additional complex component,

$$\dot{\theta}_i = \omega_i + \frac{\Gamma}{2N_G} \sum_{j=1}^{2N_G} \mathcal{R}_{ij} [\sin(\theta_j - \theta_i) - i \cos(\theta_j - \theta_i)], \quad (\text{D.1})$$

leading to

$$i\dot{\theta}_i = i\omega_i + \frac{\Gamma}{2N_G} e^{-i\theta_i} \sum_{j=1}^{N_{\text{QL}}} \mathcal{R}_{ij} e^{i\theta_j}. \quad (\text{D.2})$$

Equation (D.2) can be expressed in matrix form as

$$\frac{d}{dt} e^{i\theta} = \left[\text{diag}(i\omega) + \frac{\Gamma}{2N_G} \mathcal{R} \right] e^{i\theta} \quad (\text{D.3})$$

or, more compactly as, $\dot{\mathbf{x}} = \tilde{\mathcal{R}}\mathbf{x}$, where $\mathbf{x} = e^{i\theta} = (e^{i\theta_1}, \dots, e^{i\theta_{2N_G}})^\top$ and $\tilde{\mathcal{R}} = \text{diag}(i\omega) + \frac{\Gamma}{2N_G} \mathcal{R}$. This allows us to obtain as a closed form for the solution of the dynamics of the Kuramoto model

$$\mathbf{x}(t) = e^{\tilde{\mathcal{R}}t} \mathbf{x}(0). \quad (\text{D.4})$$

We can decompose the real and imaginary part of the frequency vector $\boldsymbol{\theta} = \boldsymbol{\theta}_{\text{re}} + i\boldsymbol{\theta}_{\text{im}}$, to obtain as a physical solution of Eq. (D.1)

$$i\boldsymbol{\theta}_{\text{re}}(t) - \boldsymbol{\theta}_{\text{im}}(t) = \log \left[e^{\tilde{\mathcal{R}}t} \mathbf{x}(0) \right], \quad (\text{D.5})$$

or

$$\boldsymbol{\theta}_{\text{re}}(t) = \text{Im} \left\{ \log \left[e^{\tilde{\mathcal{R}}t} \mathbf{x}(0) \right] \right\}, \quad (\text{D.6a})$$

$$\boldsymbol{\theta}_{\text{im}}(t) = -\text{Re} \left\{ \log \left[e^{\tilde{\mathcal{R}}t} \mathbf{x}(0) \right] \right\}. \quad (\text{D.6b})$$

¹K. Zhang, P. Rao, K. Yu, H. Lim, and V. Korepin, "Implementation of efficient quantum search algorithms on NISQ computers," *Quantum Inf. Process.* **20**, 233 (2021).

²M. Cerezo, A. Arrasmith, R. Babbush, S. C. Benjamin, S. Endo, K. Fujii, J. R. McClean, K. Mitarai, X. Yuan, L. Cincio, and P. J. Coles, "Variational quantum algorithms," *Nat. Rev. Phys.* **3**, 625–644 (2021).

³S. Sun, L.-C. Shih, and Y.-C. Cheng, "Efficient quantum simulation of open quantum system dynamics on noisy quantum computers," *Phys. Scr.* **99**, 035101 (2024).

- ⁴M. E. Beverland, P. Murali, M. Troyer, K. M. Svore, T. Hoefler, V. Kliuchnikov, G. H. Low, M. Soeken, A. Sundaram, and A. Vashillo, "Assessing requirements to scale to practical quantum advantage," [arXiv:2211.07629](#) (2022).
- ⁵J. Preskill, "Quantum Computing in the NISQ era and beyond," *Quantum* **2**, 79 (2018).
- ⁶J. W. Z. Lau, K. H. Lim, H. Shrotriya, and L. C. Kwek, "NISQ computing: where are we and where do we go?" *AAPPS Bulletin* **32**, 27 (2022).
- ⁷S. S. Gill, A. Kumar, H. Singh, M. Singh, K. Kaur, M. Usman, and R. Buyya, "Quantum computing: A taxonomy, systematic review and future directions," *Softw. - Pract. Exp.* **52**, 66–114 (2022).
- ⁸J. Tindall, M. Fishman, E. M. Stoudenmire, and D. Sels, "Efficient Tensor Network Simulation of IBM's Eagle Kicked Ising Experiment," *PRX Quantum* **5**, 010308 (2024).
- ⁹F. S. Gharehchopogh, "Quantum-inspired metaheuristic algorithms: comprehensive survey and classification," *Artif. Intell. Rev.* **56**, 5479–5543 (2023).
- ¹⁰G. D. Scholes, "Graphs that predict exciton delocalization," [arXiv preprint](#) (2025).
- ¹¹M. Krebs and A. Shaheen, *Expander families and Cayley graphs: a beginner's guide* (Oxford University Press, New York, 2011).
- ¹²A. Brouwer and W. Haemers, *Spectra of Graphs* (Springer, New York, 2011).
- ¹³G. D. Scholes, "Polaritons and excitons: Hamiltonian design for enhanced coherence," *Proc. R. Soc. A: Math. Phys. Eng. Sci.* **476**, 20200278 (2020).
- ¹⁴G. D. Scholes, "Large Coherent States Formed from Disordered k-Regular Random Graphs," *Entropy* **25**, 1519 (2023).
- ¹⁵G. D. Scholes, "Quantum-like states on complex synchronized networks," *Proc. R. Soc. A: Math. Phys. Eng. Sci.* **480**, 20240209 (2024).
- ¹⁶G. D. Scholes and G. Amati, "Quantum-like product states constructed from classical networks," *Physical Review Letters* (2025), in press, [arXiv:2406.19221](#).
- ¹⁷H. Haken, "Cooperative phenomena in systems far from thermal equilibrium and in nonphysical systems," *Rev. Mod. Phys.* **47**, 67–121 (1975).
- ¹⁸U. Fano, "A common mechanism of collective phenomena," *Rev. Mod. Phys.* **64**, 313–319 (1992).
- ¹⁹S. Strogatz, *Sync: How Order Emerges from Chaos In the Universe, Nature, and Daily Life* (Hachette Books, New York, 2012).
- ²⁰O. Artime and M. De Domenico, "From the origin of life to pandemics: emergent phenomena in complex systems," *Philos. Transact. A Math. Phys. Eng. Sci.* **380**, 20200410 (2022).
- ²¹Y. Kuramoto, "Self-entrainment of a population of coupled nonlinear oscillators," in *International Symposium on Mathematical Problems in Theoretical Physics*, edited by H. Araki (Springer Berlin Heidelberg, Berlin, Heidelberg, 1975) pp. 420–422.
- ²²Y. Kawamura, H. Nakao, K. Arai, H. Kori, and Y. Kuramoto, "Phase synchronization between collective rhythms of globally coupled oscillator groups: noiseless nonidentical case," *Chaos* **20**, 043110 (2010).
- ²³G. D. Scholes, "The Kuramoto–Lohe model and collective absorption of a photon," *Proc. R. Soc. A: Math. Phys. Eng. Sci.* **478**, 20220377 (2022).
- ²⁴F. A. Rodrigues, T. K. D. Peron, P. Ji, and J. Kurths, "The Kuramoto model in complex networks," *Phys. Rep.* **610**, 1–98 (2016).
- ²⁵A. Khrennikov, "Can Quantum Information be Processed by Macroscopic Systems?" *Quantum Inf. Process.* **6**, 401–429 (2007).
- ²⁶A. Khrennikov, "Get Rid of Nonlocality from Quantum Physics," *Entropy* **21**, 806 (2019).
- ²⁷A. Khrennikov, *Ubiquitous quantum structure* (Springer–Verlag, Berlin Heidelberg, 2010).
- ²⁸R. Diestel, *Graph Theory* (Springer, Hamburg, 2017).
- ²⁹G. D. Scholes, C. A. DelPo, and B. Kudisch, "Entropy Reorders Polariton States," *J. Phys. Chem. Lett.* **11**, 6389–6395 (2020).
- ³⁰A. Lubotzky, "Expander graphs in pure and applied mathematics," *Bull. Am. Math. Soc.* **49**, 113–162 (2012).
- ³¹B. D. McKay, "The expected eigenvalue distribution of a large regular graph," *Linear Algebra Appl.* **40**, 203–216 (1981).
- ³²I. J. Farkas, I. Derényi, A.-L. Barabási, and T. Vicsek, "Spectra of "real-world" graphs: Beyond the semicircle law," *Phys. Rev. E* **64**, 026704 (2001).
- ³³Z. Hou, H. Zhu, G.-Y. Xiang, C.-F. Li, and G.-C. Guo, "Error-compensation measurements on polarization qubits," *J. Opt. Soc. Am. B* **33**, 1256–1265 (2016).
- ³⁴A. Bengtsson, A. Opremcak, M. Khezri, D. Sank, A. Bourassa, K. J. Satzinger, S. Hong, C. Erickson, B. J. Lester, K. C. Miao, A. N. Korotkov, J. Kelly, Z. Chen, and P. V. Klimov, "Model-Based Optimization of Superconducting Qubit Readout," *Phys. Rev. Lett.* **132**, 100603 (2024).
- ³⁵L. Funcke, T. Hartung, K. Jansen, S. Kühn, P. Stornati, and X. Wang, "Measurement error mitigation in quantum computers through classical bit-flip correction," *Phys. Rev. A* **105**, 062404 (2022).
- ³⁶M. Gupta and M. J. Nene, "Quantum computing: A measurement and analysis review," *Concurr. Comput. Pract. Exp.* **33**, e6344 (2021).
- ³⁷S. Resch and U. R. Karpuzcu, "Benchmarking Quantum Computers and the Impact of Quantum Noise," **54** (2021), 10.1145/3464420.
- ³⁸S. Bravyi, S. Sheldon, A. Kandala, D. C. McKay, and J. M. Gambetta, "Mitigating measurement errors in multiqubit experiments," *Phys. Rev. A* **103**, 042605 (2021).
- ³⁹H. Ali, J. Marques, O. Crawford, J. Majaniemi, M. Serra-Peralta, D. Byfield, B. Varbanov, B. M. Terhal, L. DiCarlo, and E. T. Campbell, "Reducing the error rate of a superconducting logical qubit using analog readout information," *Phys. Rev. Appl.* **22**, 044031 (2024).
- ⁴⁰L. Basnarkov and V. Urumov, "Phase transitions in the Kuramoto model," *Phys. Rev. E* **76**, 057201 (2007).
- ⁴¹X. Wang, C. Xu, and Z. Zheng, "Phase transition and scaling in Kuramoto model with high-order coupling," *Nonlinear Dyn.* **103**, 2721–2732 (2021).
- ⁴²A. Allam, I. M. Filanovsky, L. B. Oliveira, and J. R. Fernandes, "Synchronization of mutually coupled LC-oscillators," in *2006 IEEE International Symposium on Circuits and Systems* (IEEE, 2006) pp. 4–pp.
- ⁴³I. Barbi, "Exact analysis of spontaneous phase synchronization of two identical coupled electrical linear LC oscillators," *Revista Brasileira de Ensino de Física* **43**, e20210126 (2021).
- ⁴⁴P. Maffezzoni, B. Bahr, Z. Zhang, and L. Daniel, "Oscillator Array Models for Associative Memory and Pattern Recognition," *IEEE Trans. Circuits Syst. I Regul. Pap.* **62**, 1591–1598 (2015).
- ⁴⁵A. Raychowdhury, A. Parihar, G. H. Smith, V. Narayanan, G. Csaba, M. Jerry, W. Porod, and S. Datta, "Computing With Networks of Oscillatory Dynamical Systems," *Proc. IEEE* **107**, 73–89 (2019).
- ⁴⁶A. D. Belanovsky, N. Locatelli, P. N. Skirdkov, F. Abreu Araujo, K. A. Zvezdin, J. Grollier, V. Cros, and A. K. Zvezdin, "Numerical and analytical investigation of the synchronization of dipolarly coupled vortex spin-torque nano-oscillators," *Appl. Phys. Lett.* **103**, 122405 (2013).
- ⁴⁷T. Kanao, H. Suto, K. Mizushima, H. Goto, T. Tanamoto, and T. Nagasawa, "Reservoir Computing on Spin-Torque Oscillator Array," *Phys. Rev. Appl.* **12**, 024052 (2019).
- ⁴⁸V. Flovik, F. Macià, and E. Wahlström, "Describing synchronization and topological excitations in arrays of magnetic spin torque oscillators through the Kuramoto model," *Sci. Rep.* **6**, 32528 (2016).
- ⁴⁹H.-T. Kim, B.-J. Kim, S. Choi, B.-G. Chae, Y. W. Lee, T. Driscoll, M. M. Qazilbash, and D. N. Basov, "Electrical oscillations induced by the metal-insulator transition in VO₂," *J. Appl. Phys.* **107**, 023702 (2010).
- ⁵⁰A. Parihar, N. Shukla, S. Datta, and A. Raychowdhury, "Synchronization of pairwise-coupled, identical, relaxation oscillators,"

- tors based on metal-insulator phase transition devices: A model study,” *J. Appl. Phys.* **117**, 054902 (2015).
- ⁵¹M. J. Cotter, Y. Fang, S. P. Levitan, D. M. Chiarulli, and V. Narayanan, “Computational Architectures Based on Coupled Oscillators,” in *2014 IEEE Computer Society Annual Symposium on VLSI* (2014) pp. 130–135.
- ⁵²D. M. Greenberger, M. A. Horne, and A. Zeilinger, “Going beyond Bell’s theorem,” in *Bell’s theorem, quantum theory and conceptions of the universe* (Springer, 1989) pp. 69–72.
- ⁵³M. Erhard, M. Krenn, and A. Zeilinger, “Advances in high-dimensional quantum entanglement,” *Nat. Rev. Phys.* **2**, 365–381 (2020).
- ⁵⁴D. G. Scholes, “Dynamics in an emergent quantum-like state space generated by a hidden classical system,” (2025) in preparation.
- ⁵⁵A. Khrennikov, “Representation of the Kolmogorov model having all distinguishing features of quantum probabilistic model,” *Phys. Lett. A* **316**, 279–296 (2003).
- ⁵⁶A. Shiryaev and S. Wilson, *Probability*, Graduate Texts in Mathematics (Springer, New York, 2013).
- ⁵⁷A. Kolmogoroff, “Grundbegriffe der Wahrscheinlichkeitsrechnung,” (1933).
- ⁵⁸N. Bohr, *The Philosophical Writings of Niels Bohr* (Ox Bow Press, Woodbridge, Conn., 1987).
- ⁵⁹A. Khrennikov and S. Kozyrev, “Contextual Quantization and the Principle of Complementarity of Probabilities,” *Open Syst. Inf. Dyn.* **12**, 303–318 (2005).
- ⁶⁰A. Khrennikov, “Contextuality, complementarity, signaling, and Bell tests,” *Entropy* **24**, 1380 (2022).
- ⁶¹A. Y. Khrennikov, “A Formula of Total Probability with the Interference Term and the Hilbert Space Representation of the Contextual Kolmogorovian Model,” *Theory Probab. Appl.* **51**, 427–441 (2007).
- ⁶²A. Bulinski and A. Khrennikov, “Nonclassical total probability formula and quantum interference of probabilities,” *Stat. Probab. Lett.* **70**, 49–58 (2004).
- ⁶³A. Khrennikov, “Roots of quantum computing supremacy: superposition, entanglement, or complementarity?” *Eur. Phys. J.: Spec. Top.* **230**, 1053–1057 (2021).
- ⁶⁴F. A. Pollock, C. Rodríguez-Rosario, T. Frauenheim, M. Paternostro, and K. Modi, “Operational Markov Condition for Quantum Processes,” *Phys. Rev. Lett.* **120**, 040405 (2018).
- ⁶⁵G. A. L. White, C. D. Hill, F. A. Pollock, L. C. L. Hollenberg, and K. Modi, “Demonstration of non-Markovian process characterisation and control on a quantum processor,” *Nat. Commun.* **11**, 6301 (2020).
- ⁶⁶G. D. Berk, S. Milz, F. A. Pollock, and K. Modi, “Extracting quantum dynamical resources: consumption of non-Markovianity for noise reduction,” *Npj Quantum Inf.* **9**, 104 (2023).
- ⁶⁷F. A. Pollock, C. Rodríguez-Rosario, T. Frauenheim, M. Paternostro, and K. Modi, “Non-Markovian quantum processes: Complete framework and efficient characterization,” *Phys. Rev. A* **97**, 012127 (2018).
- ⁶⁸G. Amati, J. R. Mannouch, and J. O. Richardson, “Detailed balance in mixed quantum–classical mapping approaches,” *J. Chem. Phys.* **159**, 214114 (2023).
- ⁶⁹G. Amati, J. E. Runeson, and J. O. Richardson, “On detailed balance in nonadiabatic dynamics: From spin spheres to equilibrium ellipsoids,” *J. Chem. Phys.* **158**, 064113 (2023).
- ⁷⁰J. E. Runeson, J. R. Mannouch, G. Amati, M. R. Fiechter, and J. Richardson, “Spin-mapping methods for simulating ultrafast nonadiabatic dynamics,” *Chimia* **76**, 582–588 (2022).
- ⁷¹G. Amati, M. A. C. Saller, A. Kelly, and J. O. Richardson, “Quasiclassical approaches to the generalized quantum master equation,” *J. Chem. Phys.* **157**, 234103 (2022).
- ⁷²J. R. Mannouch and J. O. Richardson, “A mapping approach to surface hopping,” *J. Chem. Phys.* **158**, 104111 (2023).
- ⁷³G. Amati, “Dynamical signatures of non-Markovianity in a dissipative-driven qubit,” *Phys. Rev. A* **109**, 052433 (2024).
- ⁷⁴M. A. M. de Aguiar, “Generalized frustration in the multidimensional Kuramoto model,” *Phys. Rev. E* **107**, 044205 (2023).
- ⁷⁵M. Lohe, “Non-Abelian Kuramoto models and synchronization,” *J. Phys. A: Math. Theor.* **42**, 395101 (2009).
- ⁷⁶M. Di Ventra and F. L. Traversa, “Perspective: Memcomputing: Leveraging memory and physics to compute efficiently,” *Appl. Phys.* **123**, 180901 (2018).
- ⁷⁷F. L. Traversa, C. Ramella, F. Bonani, and M. D. Ventra, “Memcomputing *NP*-complete problems in polynomial time using polynomial resources and collective states,” *Sci. Adv.* **1**, e1500031 (2015).
- ⁷⁸M. Di Ventra, “MemComputing vs. Quantum Computing: some analogies and major differences,” in *2022 IEEE Int. Conf. Nanotechnol.* (2022) pp. 409–412.
- ⁷⁹S. Nakajima, “On Quantum Theory of Transport Phenomena: Steady Diffusion,” *Prog. Theor. Phys.* **20**, 948–959 (1958).
- ⁸⁰H. Mori, “Transport, Collective Motion, and Brownian Motion,” *Prog. Theor. Phys.* **33**, 423–455 (1965).
- ⁸¹R. Zwanzig, “Ensemble Method in the Theory of Irreversibility,” *J. Chem. Phys.* **33**, 1338–1341 (1960).
- ⁸²J. M. Dominy and D. Venturi, “Duality and conditional expectations in the Nakajima-Mori-Zwanzig formulation,” *J. Math. Phys.* **58**, 082701 (2017).
- ⁸³G. Amati, H. Meyer, and T. Schilling, “Memory Effects in the Fermi–Pasta–Ulam Model,” *J. Stat. Phys.* **174**, 219–257 (2019).
- ⁸⁴O. Ezratty, “Perspective on superconducting qubit quantum computing,” *Eur. Phys. J. A* **59**, 94 (2023).
- ⁸⁵J. Ikonen, J. Salmilehto, and M. Möttönen, “Energy-efficient quantum computing,” *npj Quantum Inf.* **3**, 17 (2017).
- ⁸⁶A. Paler and R. Basmadjian, “Energy cost of quantum circuit optimisation: Predicting that optimising Shor’s algorithm circuit uses 1 GWh,” *ACM Trans. Quantum Comput.* **3**, 1–14 (2022).
- ⁸⁷V. Sood and R. P. Chauhan, “Quantum computing: Impact on energy efficiency and sustainability,” *Expert Syst. Appl.* **255**, 124401 (2024).
- ⁸⁸D. Jaschke and S. Montangero, “Is quantum computing green? An estimate for an energy-efficiency quantum advantage,” *Quantum Sci. Technol.* **8**, 025001 (2023).
- ⁸⁹A. Auffèves, “Quantum Technologies Need a Quantum Energy Initiative,” *PRX Quantum* **3**, 020101 (2022).
- ⁹⁰A. Khrennikov, “Quantum Bayesianism as the basis of general theory of decision-making,” *Philos. trans., Math. Phys. Eng. Sci.* **374**, 20150245 (2016).
- ⁹¹M. Ozawa and A. Khrennikov, “Application of theory of quantum instruments to psychology: Combination of question order effect with response replicability effect,” *Entropy* **22**, 37 (2020).
- ⁹²D. Widdows, J. Rani, and E. M. Pothos, “Quantum circuit components for cognitive decision-making,” *Entropy* **25**, 548 (2023).
- ⁹³A. Pal, Z. Chai, J. Jiang, W. Cao, M. Davies, V. De, and K. Banerjee, “An ultra energy-efficient hardware platform for neuromorphic computing enabled by 2D-TMD tunnel-FETs,” *Nat. Commun.* **15**, 3392 (2024).
- ⁹⁴L. Muller, J. Mináč, and T. T. Nguyen, “Algebraic approach to the Kuramoto model,” *Phys. Rev. E* **104**, L022201 (2021).